Journal of Quantitative Spectroscopy & Radiative Transfer 129 (2013) 60–68

Contents lists available at ScienceDirect

Journal of Quantitative Spectroscopy & Radiative Transfer

journal homepage: www.elsevier.com/locate/jqsrt

Journal of
Quantitative
Spectroscopy &
Radiative
Transfer

Optical characteristics of Er^{3+} ion in Er/Yb:LiNbO$_3$ crystal: Comparison with the dissimilar effect of anti-photorefractive ions Zn^{2+}, In^{3+} and Zr^{4+}

Yannan Qian [a], Rui Wang [b,*], Biao Wang [a,*], Chao Xu [b], Wei Xu [b], Lili Xing [b], Yanling Xu [b]

[a] School of Physics and Engineering, Sun Yat-sen University, Guangzhou 510275, China
[b] Department of Chemistry, Harbin Institute of Technology, Harbin 150001, China

ARTICLE INFO

Article history:
Received 18 October 2012
Received in revised form
28 May 2013
Accepted 30 May 2013
Available online 6 June 2013

Keywords:
Er:LiNbO$_3$ crystal
Anti-photorefractive ion
Emission spectra
Judd–Ofelt
McCumber and Füchtbauer–Ladenburg

ABSTRACT

The different influences of Zn^{2+}, In^{3+} and Zr^{4+} ions on the optical characteristics of Er^{3+} ion in Er/Yb:LiNbO$_3$ crystals were discussed. An enhanced 1.54 μm emission was observed for Zr/Er/Yb:LiNbO$_3$ crystal, but the Zn^{2+} tri-doping resulted in a decreased one, and the intensity of 1.54 μm emission remained about same in In/Er/Yb:LiNbO$_3$ crystal. The populations of the green emitting $^4S_{3/2}/^2H_{11/2}$ states were achieved through the three-, two- and two-phonon processes in Zn/Er/Yb:LiNbO$_3$, In/Er/Yb:LiNbO$_3$ and Zr/Er/Yb:LiNbO$_3$ crystals, respectively. Zn^{2+} and In^{3+} ions affected the optical characteristics of Er^{3+} ion via modifying the Er^{3+} ion occupancy in Er/Yb:LiNbO$_3$ crystal. The formation of $\mathrm{Er}_{\mathrm{Li}}^{2+}$–$\mathrm{Er}_{\mathrm{Nb}}^{2-}$ ion pairs caused by the Zn^{2+} and In^{3+} ions could increase the rate of cross relaxation process. The OH$^-$ absorption spectra showed that the incorporation of Zr^{4+} ions increased OH$^-$ content, which increased the probability of the nonradiative relaxation process of $^4I_{11/2} \rightarrow {}^4I_{13/2}$ (Er) in Zr/Er/Yb:LiNbO$_3$ crystal. The J–O intensity parameters Ω_t ($t = 2$, 4 and 6), the radiative lifetime (τ_{rad}) and fluorescence branching ratio (β) in Zr/Er/Yb:LiNbO$_3$ crystal were predicted by Judd–Ofelt theory. Füchtbauer–Ladenburg and McCumber methods were carried out to calculate the emission cross-sections at 1.54 μm emission. The gain cross-section, estimated as a function of the population inversion ratio, allowed us to evaluate a potential laser performance of Zr/Er/Yb:LiNbO$_3$ crystal.

1. Introduction

Erbium doped lithium niobate (Er:LiNbO$_3$) crystal, emitting Stokes or anti-Stokes luminescence, plays an important role in the applications of lasers, biological imaging, infrared detection, and solar cells [1–3]. In particular, the standard telecommunication wavelength at 1.54 μm, arising from the $^4I_{13/2} \rightarrow {}^4I_{15/2}$ transition of Er^{3+} ion, matches well the "windows of transparency" [4]. Er:LiNbO$_3$ crystal has been used as one of most promising host materials to meet the requirement of integration and miniaturization, since it could combine the lasing characteristics of Er^{3+} ion with the electro-optic and nonlinear optical properties of LiNbO$_3$ crystal [5,6].

The photorefractive effect, inducing the birefringence changes at high laser intensities, limits the performance of Er:LiNbO$_3$ crystal. Until now, comprehensive studies on the suppression of the photorefractive effect in Er:LiNbO$_3$ crystal have been investigated. It has been found that codoping with anti-photorefractive ions, such as Mg^{2+}, Zn^{2+} and In^{3+}, not only improves the photorefractive effect

---

[*] Corresponding authors.
E-mail addresses: wangrui001@hit.edu.cn (R. Wang), wangbiao@mail.sysu.edu.cn (B. Wang).

0022-4073/$ - see front matter © 2013 Elsevier Ltd. All rights reserved.
http://dx.doi.org/10.1016/j.jqsrt.2013.05.031

but also tunes the intensity of Stokes or anti-Stokes luminescence in Er:LiNbO$_3$ crystal. Sun and Zhang reported that MgO, ZnO and In$_2$O$_3$ codoping could enhance the 1.54 μm emission and simultaneously suppress the green upconversion (UC) emission in Er:LiNbO$_3$ crystal [7–10]. The J–O intensity parameters Ω_t (t=2, 4 and 6), the radiative lifetime (τ_{rad}) and fluorescence branching ratios (β) of Er:LiNbO$_3$ crystals codoped with Zn^{2+}, Mg^{2+}, In^{3+}, Sc^{3+} and Hf^{4+} ions have been calculated and discussed by Judd–Ofelt (J–O) theory [10–14]. Although breakthroughs in the optical characteristics of Er^{3+} ion in Er:LiNbO$_3$ crystals codoped with these conventional anti-photorefractive ions have been gained, their high threshold concentrations constitute still the main limitation for the crystal of good optical quality [15–18]. Therefore, Zr^{4+} ion, which has a low doping threshold (2.0 mol%) and a distribution coefficient close to 1 [19], will become the most promising anti-photorefractive ion. It is generally accepted that Yb^{3+} ion is used as a sensitizer to generate highly efficient Stokes or anti-Stokes luminescence in Er^{3+}-doped host materials under 980 nm excitation. This is because Yb^{3+} ion has a large absorption cross-section around 980 nm wavelength and can transfer efficiently its energy to Er^{3+} ion [20,21]. Recently, spectroscopic characteristics of Er^{3+} ion in Er/Yb:LiNbO$_3$ crystals tri-doped with Zn^{2+} and In^{3+} ions have been discussed based on J–O theory [22,23]. However, to our knowledge, there are no detailed works on the spectroscopic analysis of Zr/Er/Yb:LiNbO$_3$ crystal. Moreover, it is unclear that if the different effect of Zn^{2+}, In^{3+} and Zr^{4+} ions on the optical characteristics of Er^{3+} ion would be observed in Er/Yb:LiNbO$_3$ crystal.

In this paper, Er^{3+} (1 mol%)/Yb^{3+} (1 mol%):LiNbO$_3$ crystals tri-doped without and with Zr^{4+} ions were grown by the Czochralski technique. For a comparison, the upconversion and near infrared emission spectra of Zn/Er/Yb:LiNbO$_3$ and In/Er/Yb:LiNbO$_3$ crystals grown by the Czochralski technique have been investigated. The OH$^-$ absorption spectra of Er/Yb:LiNbO$_3$ and Zr/Er/Yb:LiNbO$_3$ crystals were studied. The intensity parameters Ω_t (t=2, 4 and 6), the radiative lifetime (τ_{rad}) and fluorescence branching ratio (β) in Zr/Er/Yb:LiNbO$_3$ crystal were calculated by J–O theory. McCumber and Füchtbauer–Ladenburg methods were used to discuss the emission cross-section spectra of 1.54 μm emission, as well as the gain cross-section spectrum for the $^4I_{13/2}\rightarrow{}^4I_{15/2}$ transition was also analyzed.

2. Experimental

Congruent ([Li]/[Nb]=0.946) Er/Yb:LiNbO$_3$ crystals tri-doped with ZnO, In$_2$O$_3$ and ZrO$_2$ were grown by the Czochralski technique. The purities of the raw materials Li$_2$CO$_3$, Nb$_2$O$_5$, Er$_2$O$_3$, Yb$_2$O$_3$, ZnO, In$_2$O$_3$ and ZrO$_2$ were 99.99%. The mixtures, which were mixed for 24 h, were heated at 750 °C for 2 h to remove CO$_2$ and then formed polycrystalline powder via heating up to 1150 °C for 2 h. The optimum technology conditions of crystal growth were the axial temperature gradient of 40–50 K/cm, the rotating rate of 10–25 rpm and the pulling rate of 0.5–2 mm/h. The grown crystals were polarized at 1200 °C with a current density of 5 mA/cm^2. The polarized crystals were cut into Y-plates ($X\times Y\times Z\approx 10\times 2\times 10$ mm^3) with optically polished surfaces. The compositions of these grown crystals are listed in Table 1.

Table 1
Compositions of the crystals in the melt.

Sample no.	Er^{3+}	Yb^{3+}	Zn^{2+}	In^{3+}	Zr^{4+}
	(X mol%)				
Er/Yb-0.5	0.5	0.5	0	0	0
Er/Yb-1	1.0	1.0	0	0	0
Zn/Er/Yb:LN	0.5	0.5	5.0	0	0
In/Er/Yb:LN	0.5	0.5	0	2.0	0
Zr/Er/Yb:LN	1.0	1.0	0	0	2.0

The inductively coupled plasma mass spectrometry (ICP-MS, Optima 7500 Series, Agilent Technologies Inc, Beijing) was used to determined the Er^{3+} ion content ([Er^{3+}]/[Nb^{5+}] ratio) in the crystal, and the obtained concentrations of Er^{3+} ion in Zr/Er/Yb:LN, Er/Yb-1 and Zn/Er/Yb:LN crystals were 2.719×10^{20} cm^{-3}, 2.832×10^{20} cm^{-3} and 1.416×10^{20} cm^{-3}, respectively. The power-controllable diode laser, operating at 980 nm wavelength, was used to measure the near infrared and upconversion emission spectra. All fluorescence emission spectra were recorded at the same geometry by using the spectrometer (Bruker optics 500IS/SM) equipped with a semiconductor cooled charge coupled device detector (DV440, Andor). The Fourier-Transform spectrophotometer (Niconet-710, Nicolet, USA) was used to measure the OH$^-$ absorption spectra. The UV–vis-near infrared absorption spectra in the range from 300 to 1650 nm were measured by the CARY spectrophotometer.

3. Results

3.1. Optical characteristics of Er^{3+} ion

Fig. 1 shows the near infrared emission spectra of Er/Yb-0.5, Er/Yb-1, Zn/Er/Yb:LN, In/Er/Yb:LN and Zr/Er/Yb:LN crystals under 980 nm excitation. The near infrared emission centered at 1540 nm corresponds to the $^4I_{13/2}\rightarrow{}^4I_{15/2}$ transition of Er^{3+} ion. It is can be seen from Fig. 1A that Zr/Er/Yb:LN presents the 1.54 μm emission about 3 times stronger than Er/Yb-1 crystal, which favors to meet the requirement of broadband amplification and lasing around 1.54 μm wavelength. As illustrated in Fig. 1B and C, the intensity of 1.54 μm emission remains about the same in In/Er/Yb:LN, while the introduction of Zn^{2+} ions leads to a drastically decreased 1.54 μm emission in Zn/Er/Yb:LN crystal.

The UC emission spectra of Er/Yb:LiNbO$_3$ crystals tri-doped with Zn^{2+}, In^{3+} and Zr^{4+} ions under 980 nm excitation are displayed in Fig. 2. The strong emission peaks at 525/550 nm are assigned to the $^2H_{11/2}/^4S_{3/2}\rightarrow{}^4I_{15/2}$ transitions of Er^{3+} ion, respectively, and a weak red emission peak at 660 nm corresponds to the $^4F_{9/2}\rightarrow{}^4I_{15/2}$ transition [24]. As shown in Fig. 2A and B, the intensity of green UC emission increases with the incorporation of Zn^{2+} ions, whereas decreases with the tri-doping with In^{3+} ions. As for

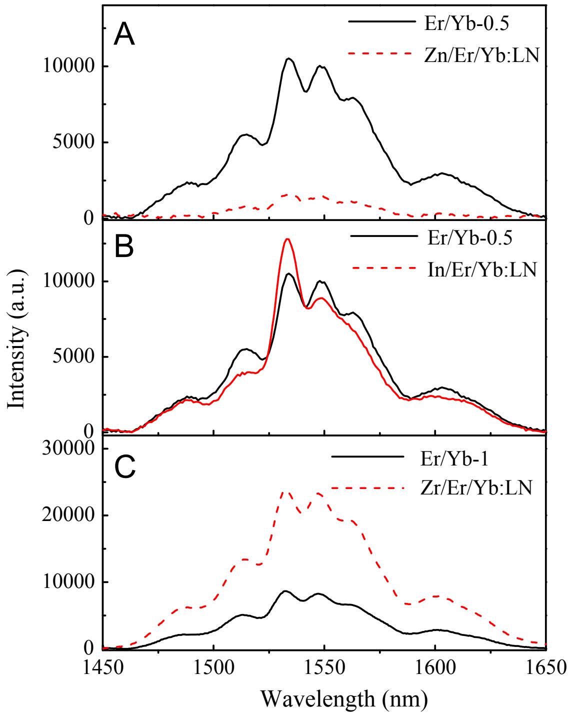

Fig. 1. The near infrared emission spectra of Er/Yb:LiNbO$_3$ crystals tri-doped with Zn^{2+}, In^{3+} and Zr^{4+} ions under 980 nm excitation.

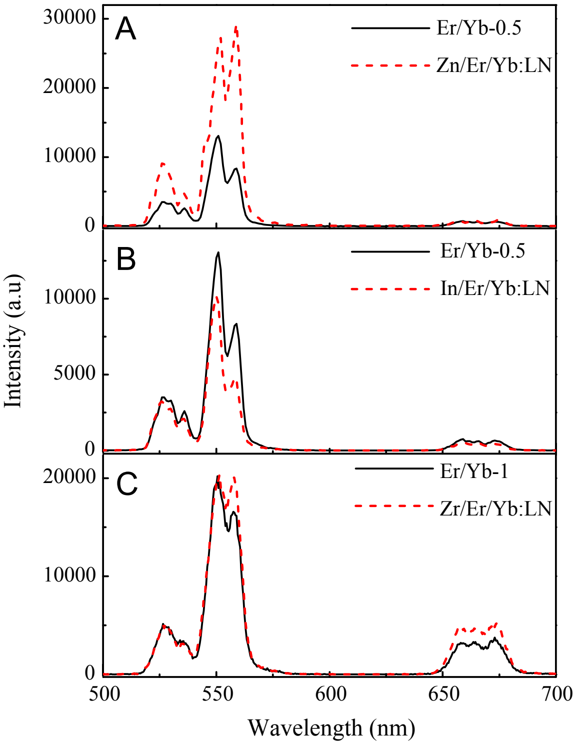

Fig. 2. The upconversion emission spectra of Er/Yb:LiNbO$_3$ crystals tri-doped with Zn^{2+}, In^{3+} and Zr^{4+} ions under 980 nm excitation.

the red UC emission, the almost changeless intensities are observed for Zn/Er/Yb:LN and In/Er/Yb:LN crystals. It is can be seen from Fig. 2C that the Zr^{4+} tri-doping results in a similar intensity of green UC emission and an increase of red UC emission in Zr/Er/Yb:LN crystal.

To understand the UC mechanisms, double logarithmic plots of the fluorescence intensity (I_f) versus pump power (P) for the green and red UC emissions in Zr/Er/Yb:LN crystal are shown in Fig. 3. For an unsaturated UC process, the number of pump photons (n) required to populate the emitting state can be obtained via the formula: $I_f \propto P^n$ [25]. As seen in Fig. 3, the intensities of green and red UC emissions show a quadratic dependence on the pump power, indicating that a two-photon process has been involved in producing the green and red UC emissions in Er/Yb-1 crystal. As for the Zr/Er/Yb:LN crystal, the slope values are equal to 2.2 and 1.7 for the green and red UC emissions, respectively, which are consistent with the well known two-photon process. The fact that the n value of 1.7 for Zr/Er/Yb:LN is lower than the expected value of 2 may be due to “saturation” of the UC process. According to our previous works [22], the slope values are found to be 3.27 and 2.72 for the green and red UC emissions, respectively, in Zn/Er/Yb:LN crystal. This is an indication that the green and red UC emissions are populated via the three-photon processes in Zn/Er/Yb:LN crystal. The slope value is observed to be 1.85 for the green UC emission in In/Er/Yb:LN crystal, suggesting that a two-photon process is involved in the population of the green emitting $^4S_{3/2}/^2H_{11/2}$ states [26].

The energy levels of Er^{3+} and Yb^{3+} ions, as well as the UC mechanisms in Zn/Er/Yb:LN, In/Er/Yb:LN and Zr/Er/Yb:LN crystals are presented in Fig. 4. In the case of Er^{3+} and Yb^{3+} ions codoped host materials under 980 nm excitation, only the laser excitation of Yb^{3+} ion is considered due to its large absorption cross section around 980 nm wavelength and the efficient energy transition to Er^{3+} ion.

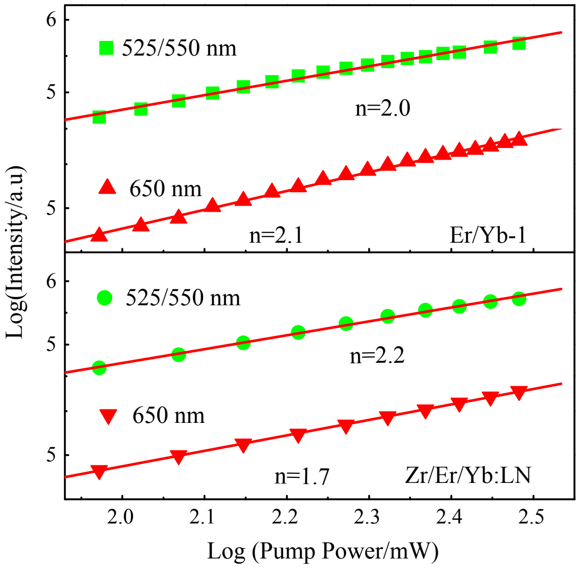

Fig. 3. Pump power dependences of upconversion emission intensity in Er/Yb-1 and Zr/Er/Yb:LN crystals under 980 nm excitation.

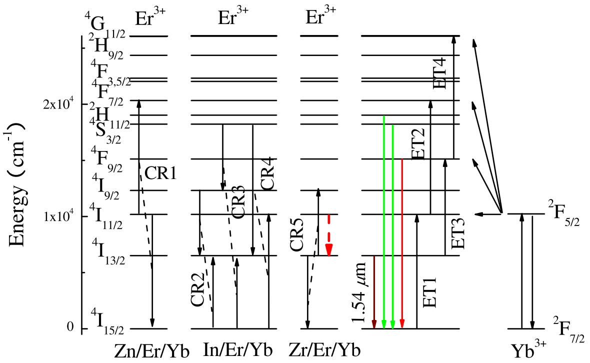

Fig. 4. The energy levels of Er^{3+} and Yb^{3+} ions and the upconversion mechanisms in Er/Yb:$LiNbO_3$ crystals tri-doped with Zn^{2+}, In^{3+} and Zr^{4+} ions.

The UC mechanisms of Zn/Er/Yb:LN and In/Er/Yb:LN crystals have been substantially depicted in the previous literatures [22,26]. The important population processes are briefly presented here. The three-photon process to populate the green emitting $^4S_{3/2}$/$^2H_{11/2}$ states in Zn/Er/Yb:LN crystal is illustrated as follows: ET1: $^4I_{15/2}$ Er+$^2F_{5/2}$ Yb→$^4I_{11/2}$ Er+$^2F_{7/2}$ Yb, ET3: $^4I_{13/2}$ Er+$^2F_{5/2}$ Yb→$^4F_{9/2}$ Er+$^2F_{7/2}$ Yb and ET4: $^4F_{9/2}$ Er+$^2F_{5/2}$ Yb→$^4G_{11/2}$ Er+$^2F_{7/2}$ Yb. Owing to the long lifetime of the $^4I_{11/2}$ state, the cross relaxation (CR) process, CR1: $^4I_{11/2}$+$^4I_{11/2}$→$^4F_{7/2}$+$^4I_{15/2}$ (Er), occurs between the two adjacent Er^{3+} ions in Zn/Er/Yb:LN crystal. A two-photon process (ET1 and ET2: $^4I_{11/2}$ Er+$^2F_{5/2}$ Yb→$^4F_{7/2}$ Er+$^2F_{7/2}$ Yb) substitutes the three-photon one to populate the green UC emission in In/Er/Yb:LN and Zr/Er/Yb:LN crystals. As for In/Er/Yb:LN crystal, there are three CR processes: CR2: $^4I_{9/2}$+$^4I_{15/2}$→$^4I_{13/2}$+$^4I_{13/2}$ (Er), CR3: $^4S_{3/2}$+$^4I_{15/2}$→$^4I_{9/2}$+$^4I_{13/2}$ (Er) and CR4: $^4S_{3/2}$+$^4I_{15/2}$→$^4I_{13/2}$+$^4I_{9/2}$ (Er). As shown in Fig. 4, different from In/Er/Yb:LN crystal, CR5 process ($^4I_{13/2}$+$^4I_{13/2}$→$^4I_{15/2}$+$^4I_{9/2}$) occurs in Zr/Er/Yb:LN crystal. It is believable that the occurrence of CR5 process may be attributed to the efficient nonradiative relaxation (NR) process from the $^4I_{11/2}$ to $^4I_{13/2}$ state of Er^{3+} ion. This behavior will be explained by the OH^- absorption spectra of Zr/Er/Yb:LN and Er/Yb-1 crystal.

The OH^- absorption spectra of Er/Yb:$LiNbO_3$ tri-doped without and with Zr^{4+} ions, shown in Fig. 5, display that the bands occurring in the wavenumber range of 3450–3550 cm^{-1} are assigned to the vibration of hydroxyl (OH^-) group. One can see that the introduction of Zr^{4+} ions leads to a considerable increase of OH^- absorption, meaning the enhanced OH^- content in Zr/Er/Yb:LN crystal. According to Fig. 4, there is a competition between the NR process of $^4I_{11/2}$→$^4I_{13/2}$ transition and ET2 process for the population of the $^4I_{11/2}$ state (Er). The rate of nonradiative relaxation process (W_{nr}) can be determined by the following expression [27]:

$$W_{nr} = C\exp\left(-\alpha\cdot\frac{\Delta E}{\hbar\omega}\right) \tag{1}$$

where C and α are constants, ΔE is the energy gap between the relaxing and the lower state, and $\hbar\omega$ is the highest phonon energy in the material. The value of $\Delta E/\hbar\omega$ represents the number of phonons (P) required to bridge ΔE. According to the above equation, W_{nr} is inversely proportional to P ($\Delta E/\hbar\omega$). The energy gap between the $^4I_{11/2}$ and $^4I_{13/2}$ state, which is about 3680 cm^{-1}, is only required one or two high frequency vibration OH^- groups to bridge. The presence of OH^- groups could reduce the number of phonons to bridge the energy gap between the $^4I_{11/2}$ and $^4I_{13/2}$ state and make the NR process drastically efficient. Consequently, the large OH^- content increases the probability of the $^4I_{11/2}$→$^4I_{13/2}$ nonradiative relaxation process and simultaneously leads to an enhanced population of the $^4I_{13/2}$ state in Zr/Er/Yb:LN crystal. After the $^4I_{13/2}$ state is largely populated, the CR5 process occurs in Zr/Er/Yb:LN crystal.

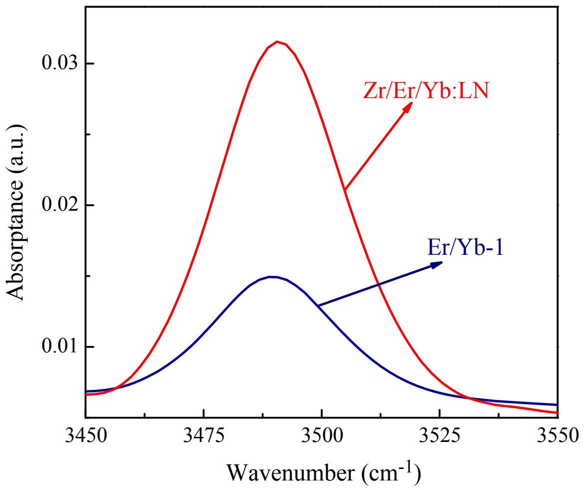

Fig. 5. The OH^- absorption spectra of Er/Yb-1 and Zr/Er/Yb:LN crystals.

Based on the Li vacancy defect model in $LiNbO_3$ crystal lattice [28], the Er^{3+} and Yb^{3+} ions occupy the Li sites and form Er_{Li}^{2+} and Yb_{Li}^{2+} defect groups, respectively. Considering the stabilization of the crystal lattice, the small discrepancy of the ionic radius between the doped ion and replaced one could decrease the degree of structural disorder. The ionic radius of Zn^{2+}, In^{3+} and Zr^{4+} ions are 0.74 Å, 0.8 Å and 0.72 Å, respectively. As Zn^{2+} and In^{3+} ions are induced into Er/Yb:$LiNbO_3$ crystals, Er^{3+} and Yb^{3+} ions are compelled to occupy Nb sites due to the following reason: the discrepancy of the ionic radius between Zn^{2+} (0.74 Å)/In^{3+} (0.8 Å) and Li^+ (0.76 Å) ion is smaller than that between Er^{3+} (0.881 Å)/Yb^{3+} (0.858 Å) and Li^+ ion. Therefore, Er_{Li}^{2+}–Er_{Nb}^{2-}, Er_{Li}^{2+}–Yb_{Nb}^{2-}, Yb_{Li}^{2+}–Er_{Nb}^{2-} and Yb_{Li}^{2+}–Yb_{Nb}^{2-} ion pairs are formed in Zn/Er/Yb:LN and In/Er/Yb:LN crystals. Since the defect stacking sequence of the $LiNbO_3$ crystal doped with the cation (M^{n+}) along c-axis can be described as $\{\ldots M_{Li}^{(n-1)+}, M_{Nb}^{(n-1)-}, \square, M_{Li}^{(n-1)+}, M_{Nb}^{(n-1)-}, \square, M_{Li}^{(n-1)+}, M_{Nb}^{(n-1)-}, \square, \ldots\}$, the distance between the Er_{Li}^{2+}–Er_{Nb}^{2-} ion pair is shorter than that between the Er_{Li}^{2+}–Er_{Li}^{2+} or Er_{Nb}^{2-}–Er_{Nb}^{2-}. It is well known that the rate of CR process is inversely proportional to the distance between two neighboring rare-earth ions. Consequently, the formation of Er_{Li}^{2+}–Er_{Nb}^{2-} ion pairs favors the efficient CR process. According to Fig. 4, the increasing CR1 process caused by the Zn^{2+} tri-doping increases the population of $^4F_{7/2}$ state and in turn depopulates the $^4I_{11/2}$ state of Er^{3+} ion. Further, the population of $^4I_{13/2}$ state (Er) decreases with the introduction of Zn^{2+} ions since the $^4I_{13/2}$ state is populated by NR process of $^4I_{11/2}$→$^4I_{13/2}$ transition.

The overall result is the observed increase of green UC emission and a decrease of 1.54 μult is the shown in Figs. 1 and 2A. The fact that the Er_{Li}^{2+}–Er_{Nb}^{2-} ion pairs formed in In/Er/Yb:LN crystal result in the increased rates of CR2, CR3 and CR4 processes is responsible for the reduction of green UC emission, in agreement with the experimental results illustrated in Fig. 2B. In contrast, the discrepancy of the ionic radius between Zr^{4+} (0.72 Å) and Li^{+} (0.76 Å) is larger than that between Zr^{4+} and Nb^{5+} (0.69 Å). Accordingly, as Zr^{4+} ions are induced into $LiNbO_3$ crystal lattice, they would like to occupy Nb sites at low doping concentration. This may explain the lower threshold concentration of Zr^{4+} ion in $LiNbO_3$ crystal. Since Zr^{4+} ions occupy Nb sites at low concentration, there is little effect of Zr^{4+} ions on the Er^{3+} ions replaced Li sites, and further on the rate of CR5 ($^4I_{13/2}$+$^4I_{13/2}\to{}^4I_{15/2}$+$^4I_{9/2}$) process. The drastic enhancement of 1.54 μm emission induced by Zr^{4+} ions arises from the efficient NR process of $^4I_{11/2}\to{}^4I_{13/2}$ transition in Zr/Er/Yb:LN crystal.

3.2. Judd–Ofelt analysis

The UV–vis-near infrared absorption spectra of Er/Yb-1 and Zr/Er/Yb:LN crystals in the range from 300 nm to 1650 nm are shown in Fig. 6. It is clear that the transitions from the $^4I_{15/2}$ ground state to the $^4G_{9/2}$, $^4G_{11/2}$, $^2H_{9/2}$, $^4F_{3/2}$, $^4F_{7/2}$, $^2H_{11/2}$, $^4S_{3/2}$, $^4F_{9/2}$ and $^4I_{13/2}$ states of Er^{3+} ion produce the absorption bands centered at 368 nm, 381 nm, 410 nm, 453 nm, 492 nm, 525 nm, 550 nm, 660 nm and 1540 nm. The 980 nm absorption band arises from the overlapping of the $^4I_{15/2}\to{}^4I_{11/2}$ transition of Er^{3+} ion and the $^2F_{7/2}\to{}^2F_{5/2}$ transition of Yb^{3+} ion.

The spectroscopic characteristics of Er^{3+} ion in Zn/Yb/Er:LN, In/Yb/Er:LN and Zr/Yb/Er:LN crystals can be understood by J–O theory which have been reported in detail in earlier Refs. [29–31]. The electric- and magnetic-dipole line strengths (S_{ed} and S_{md}) and the local field electric- and magnetic-dipole correction factor (X_{ed} and X_{md}) are given by [32]:

$$S_{ed}(J\to J') = e^2 \sum_{t=2,4,6} \Omega_t |\langle SLJ||U^{(t)}||S'L'J'\rangle|^2 \tag{2}$$

$$S_{md}(J\to J') = \left(\frac{eh}{4\pi mc}\right)^2 |\langle SLJ||\vec{L}+2\vec{S}||S'L'J'\rangle|^2 \tag{3}$$

$$X_{ed(md)} = \frac{X_{ed(md)}(n_e)+X_{ed(md)}(n_o)}{2} \tag{4}$$

where λ is the barycentre wavelength at a given absorption band; m, c and h are the mass of the electron, light speed in vacuum and Planck's constant, respectively; J and J' are the initial and final manifold, respectively. Since the value of $|\langle SLJ||U^{(t)}||S'L'J'\rangle|^2$, doubly reduced matrix elements of the unit-tensor operator $U^{(\lambda)}$, is independent on host material, its value can be obtained from Ref. [33]. It is found via Eq. (3) that the value of S_{md} for the $^4I_{15/2}\to{}^4I_{13/2}$ transition is calculated to be 69×10^{-8}. In Eq. (4), n_o and n_e are ordinary and extraordinary refractive indices of $LiNbO_3$ crystal, which could be obtained from the Sellmeier equation [34].

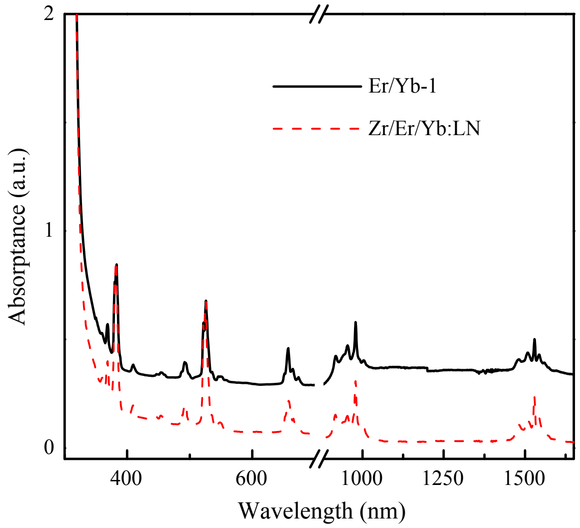

Fig. 6. The UV–vis-near infrared absorption spectra of Er/Yb-1 and Zr/Er/Yb:LN crystals.

Accordingly, the theoretical transition strength $f_{the}(J\to J')$ of Er^{3+} ion can be calculated by the following equation:

$$f_{the}(J\to J') = \frac{8\pi^2 mc}{3h(2J+1)\lambda}\left(X_{ed}\frac{S_{ed}}{e^2}+X_{md}\frac{S_{md}}{e^2}\right) \tag{5}$$

Based on the measured UV–vis-near infrared absorption spectra (Fig. 6), the experimental transition strength $f_{exp}(J\to J')$ is evaluated from:

$$f_{\exp}(J\to J') = \frac{mc^2}{N\pi e^2\lambda^2}\frac{1}{0.43d}\int OD(\lambda)d(\lambda) \tag{6}$$

where d is the thickness of the sample, $OD(\lambda)$ is the optical density and N is the number of rare earth ions per unit volume. The intensity parameters Ω_t (t=2, 4 and 6) are calculated by using a least-squares fitting in combination with Eqs. (5) and (6).

The root mean-square deviation (δ_{rms}) is used to determine the accuracy of the fitting results, and the calculated equation is given by:

$$\delta_{rms} = \left(\frac{\sum_{J'=1}^{L}(f_{\exp}-f_{the})^2}{L-3}\right)^{1/2} \tag{7}$$

where L is the number of the absorption bands involved in the fitting, f_{the} is obtained by inducing the J–O parameters Ω_t (t=2, 4 and 6) into Eq. (5).

The other important parameters, the fluorescence branching ratio (β) for the $J\to J'$ transition and the radiative lifetime (τ_{rad}), are calculated by using the obtained intensity parameters Ω_t (t=2, 4 and 6) and the following equations:

$$\tau_J = 1/\sum_{J'} A(J\to J') \tag{8}$$

$$\beta = A(J\to J')/\sum_{J'} A(J\to J') \tag{9}$$

$$A(J\to J') = \frac{4\pi^2 e^2 n^3 h}{3m^2c^2(2J+1)\lambda^3}|\langle SLJ||\vec{L}+2\vec{S}||S'L'J'\rangle|^2 + \frac{64\pi^4 e^2}{3h(2J+1)\lambda^3}\frac{n(n^2+2)^2}{9}\sum_{t=2,4,6}\Omega_t|\langle SLJ||U^{(t)}||S'L'J'\rangle|^2 \tag{10}$$

Table 2
The theoretical (f_{the}) and experimental transition strength (f_{exp}) and J–O intensity parameters Ω_t (t=2, 4 and 6) of Zr/Er/Yb:LN and Er/Yb-1 crystals. The unit is 10^{-20} cm^2 for Ω_t (t=2, 4 and 6), and the unit is 10^{-8} for f_{the} and f_{exp}.

Transition $^4I_{15/2}$ →	Er/Yb-1		Zr/Er/Yb:LN	
	f_{exp}	f_{the}	f_{exp}	f_{the}
$^4I_{13/2}$	119.269	119.206	151.341	148.187
$^4F_{9/2}$	201.082	183.353	2.524	206.256
$^4S_{3/2}$	24.803	15.489	37.103	27.927
$^2H_{11/2}$	511.195	470.628	865.948	770.407
$^4F_{7/2}$	135.024	110.485	189.329	151.590
$^4F_{3,5/2}$	45.810	31.155	72.102	56.432
$^2H_{9/2}$	55.603	32.926	75.801	51.525
$^4G_{11/2}$	903.862	926.435	1450.349	1518.602
$^4G_{9/2}$	121.597	164.099	158.696	177.800
δ_{rms} ($\times 10^{-7}$)	3.08		5.30	
Ω_2	4.16		8.10	
Ω_4	3.67		3.72	
Ω_6	0.71		1.28	

Table 3
The J–O intensity parameters Ω_t (t=2, 4 and 6) in Er/Yb:LN crystals tri-doped with Zn^{2+}, In^{3+} and Zr^{4+} ions, and those in the other Er^{3+} doped crystals.

Sample	Ω_2	Ω_4	Ω_6	Refs.
	($\times 10^{-20}$ cm^2)			
Zr/Er/Yb:LN	8.10	3.72	1.28	This work
Zn/Er/Yb:LN	7.23	3.15	1.43	[22]
In/Er/Yb:LN	9.44	5.50	2.39	[23]
$GdVO_4$	12.60	2.50	0.76	[36]
$LuVO_4$	13.28	3.04	1.60	[37]
$YAlO_3$	2.83	1.39	1.29	[38]
Lu_2SiO_5	4.45	1.61	1.16	[39]
$KGd(WO_4)_2$	8.90	0.96	0.82	[40]

where $\sum_{J'} A(J\rightarrow J')$ is the reciprocal of the total spontaneous emission probabilities, and the value of A ($J\rightarrow J'$) is named as Einstein spontaneous emission probability. In Eq. (10), the first and second terms are the electric- (A_{ed} ($J\rightarrow J'$)) and magnetic-dipole (A_{md} ($J\rightarrow J'$)) radiation, respectively.

The calculated experimental transition strengths (f_{exp}), theoretical ones (f_{the}), the root mean-square deviation (δ_{rms}) and the J–O intensity parameters Ω_t (t=2, 4 and 6) in Er/Yb-1 and Zr/Er/Yb:LN crystals are illustrated in Table 2. The parameters δ_{rms} are 5.30×10^{-7} and 3.08×10^{-7}, respectively, for Zr/Er/Yb:LN and Er/Yb-1 crystals. The similar value of δ_{rms} has been found in the previous calculated δ_{rms} in Er:$LiNbO_3$ crystal [35], suggesting the creditability of J–O intensity parameters here. It is well known that Ω_2 is dependence on the asymmetry and covalency of Er–O band. The behavior that the Zr^{4+} tri-doping increases the value of Ω_2 means Er^{3+} ion in a more polarized environment of Zr/Er/Yb:LN crystal. Since the polarization characteristic of the Er^{3+} ion is related to the Er^{3+}-site symmetries, Zr^{4+} ions modify the Er^{3+}-site symmetries and improve the 1.54 μm emission. The bulk properties and rigidity of the samples are mainly affected by Ω_4 and Ω_6. In order to understand clearly the effect of Zn^{2+}, In^{3+} and Zr^{4+} ions on the spectroscopic characteristics of Er^{3+} ion, the J-O intensity parameters Ω_t (t=2, 4 and 6) in Zn, In, Zr/Er/Yb:LN and the other Er-doped host materials are displayed in Table 3.

Table 4
The radiative lifetime (τ_{rad}) and fluorescence branching ratios (β) in Zr/Er/Yb:LN and Er/Yb-1 crystals.

Transition	Zr/Er/Yb:LN		In/Er/Yb:LN		Zn/Er/Yb:LN	
	β	τ_{rad} (μs)	β	τ_{rad} (μs)	β	τ_{rad} (μs)
$^4I_{13/2}\rightarrow{}^4I_{15/2}$	1	2659.6	1	1519.6	1	2533.4
$^4I_{11/2}\rightarrow{}^4I_{13/2}$	0.1529	1585.1	0.1400	977.1	0.1487	1527.1
$^4I_{15/2}$	0.8471		0.8600		0.8514	
$^4I_{9/2}\rightarrow{}^4I_{11/2}$	0.0054	839.0	0.0044	548.4	0.0060	950.7
$^4I_{13/2}$	0.1229		0.1484		0.1533	
$^4I_{15/2}$	0.8716		0.8472		0.8407	
$^4F_{9/2}\rightarrow{}^4I_{9/2}$	0.0138	116.8	0.0091	74.9	0.0150	128.2
$^4I_{11/2}$	0.0240		0.0258		0.0277	
$^4I_{13/2}$	0.0448		0.0428		0.0435	
$^4I_{15/2}$	0.9175		0.9223		0.9139	
$^4S_{3/2}\rightarrow{}^4F_{9/2}$	≈0	170.5	≈0	91.8	≈0	154.2
$^4I_{9/2}$	0.0422		0.0383		0.0377	
$^4I_{11/2}$	0.0196		0.0191		0.0190	
$^4I_{13/2}$	0.2552		0.2564		0.2566	
$^4I_{15/2}$	0.6826		0.6859		0.6864	
$^2H_{11/2}\rightarrow{}^4F_{9/2}$	0.0024	19.8	0.0023	16.5	0.0023	21.9
$^4I_{9/2}$	0.0098		0.0105		0.0101	
$^4I_{11/2}$	0.1728		0.1460		0.1898	
$^4I_{13/2}$	0.0132		0.0155		0.0132	
$^4I_{15/2}$	0.8018		0.8258		0.7847	
$^2H_{9/2}\rightarrow{}^4F_{7/2}$	0.0016	31.6	0.0016	24.4	0.0015	31.9
$^2H_{11/2}$	0.0044		0.0047		0.0040	
$^4F_{9/2}$	0.1486		0.1166		0.1498	
$^4I_{9/2}$	0.3339		0.2597		0.3367	
$^4I_{11/2}$	0.0765		0.0790		0.0720	
$^4I_{13/2}$	0.2537		0.2874		0.2420	
$^4I_{15/2}$	0.18123		0.2510		0.1941	

The radiative lifetimes (τ_{rad}) and fluorescence branching ratios (β) in Zn/Er/Yb:LN and Zr/Er/Yb:LN are calculated by use of Eqs. (8)–(10) and these parameters in In/Er/Yb:LN crystal have been reported in Ref. [23], which are listed in Table 4. It can be seen that the radiative lifetime (τ_{rad}) of $^4I_{13/2}$ state (Er) are 2659.6 μs, 1519.6 μs and 2533.4 μs for Zr/Er/Yb:LN, In/Er/Yb:LN and Zn/Er/Yb:LN crystals, respectively. The lengthening lifetime observed in Zr/Er/Yb:LN favors to design the practical device of 1.54 μm waveguide. The fluorescence branching ratio (β) of the $^4S_{3/2}\rightarrow{}^4I_{15/2}$ transition decreases from 0.6864 of Zn/Er/Yb:LN to 0.6826 of Zr/Er/Yb:LN crystal. The small fluorescence branching ratio (β) means the low probability of radiative transition. The small β value of 0.6823 indicates the weak green UC emission in Zr/Er/Yb:LN crystal. It is expected that the Zr^{4+} tri-doping could lead to an efficient 1.54 μm emission in Zr/Er/Yb:LN crystal, since the suppression of green UC emission is beneficial to the amplification gain at 1.54 μm emission [8].

3.3. Emission cross-section calculation

In order to predict quantitatively the performance of lasers and amplifiers, McCumber (M-C) and Füchtbauer–Ladenburg (F–L) theories are used to determine the absorption and emission cross-sections. Based on F–L theory, the emission cross-section is determined from the measured near infrared emission spectra (Fig. 1), and the calculation equation is given by [41]:

$$\sigma_{FL-em}(\lambda)=\frac{\lambda^5}{8\pi cn^2\tau}\frac{I(\lambda)}{\int\lambda I(\lambda)d\lambda} \tag{11}$$

where λ is the emission wavelength observed in the near infrared emission spectrum, τ is the radiative lifetime, and n is the refractive index.

The emission cross-section also can be obtained from the calculated absorption cross-section spectra via using the M-C relation [42]:

$$\sigma_{MC-em}(\lambda)=\sigma_{abs}(\lambda)\frac{Z_l}{Z_u}\exp\left(\frac{E_{ZL}-hc/\lambda}{kT}\right) \tag{12}$$

where h, c and k are Planck's constant, the light speed in vacuum and Boltzmann constant, respectively; the ratio of Z_l/Z_u is equal to 0.8, in which Z_l and Z_u are the partition functions for the lower and upper levels involved in the considered optical transition, respectively; E_{ZL} is the energy of the zero-line between the lowest crystal field components of the electronic states. The term $\sigma_{abs}(\lambda)$, representing the absorption cross-section, can be calculated by the following equation [43]:

$$\sigma_{abs}(\lambda)=2.303\frac{OD(\lambda)}{Nd} \tag{13}$$

where λ is the absorption wavelength, OD (λ) is the optical density, N is the concentration of Er^{3+} ion in the crystal and d is the thickness of the sample.

Fig. 7 shows the absorption and emission cross-sections for the $^4I_{13/2}\rightarrow{}^4I_{15/2}$ transition of Er^{3+} ion in Zr/Er/Yb:LN crystal. As illustrated in Fig. 7, despite the peak shapes of the two emission cross-sections are discrepancy, the values of σ_{MC-em} and σ_{FL-em} are almost same, indicating that the obtained calculated results by use of M-C and F–L theories are believable here. Based on F–L theory, the emission cross-section at 1547 nm and 1533 nm are 6.75×10^{-21} cm^2 and 6.60×10^{-21} cm^2, respectively. The emission cross-section calculated by M-C theory at 1529 nm is equal to 7.18×10^{-21} cm^2. It has been reported that the maximum σ_{em} in In/Er/Yb:LN and Zn/Er/Yb:LN crystals through F–L theory are calculated to be 17.0×10^{-21} cm^2 and 8.42×10^{-21} cm^2, respectively. Although the value of emission cross-section in Zr/Er/Yb:LN crystal is smaller than those in In/Er/Yb:LN and Zn/Er/Yb:LN crystals, it is larger than those in Er:LaGaO$_3$ ($\sigma_{em}=5.9\times10^{-21}$ cm^2) and Er:Sr$_3$Y(BO$_3$)$_3$ (4.75×10^{-21} cm^2) [44,45].

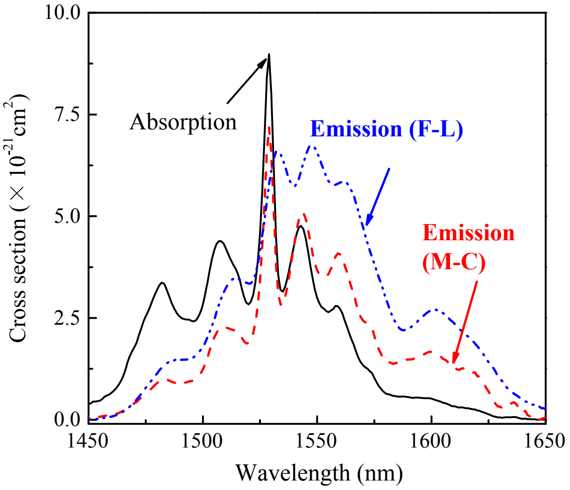

Fig. 7. The absorption and emission cross-section spectra of Zr/Er/Yb:LN crystal.

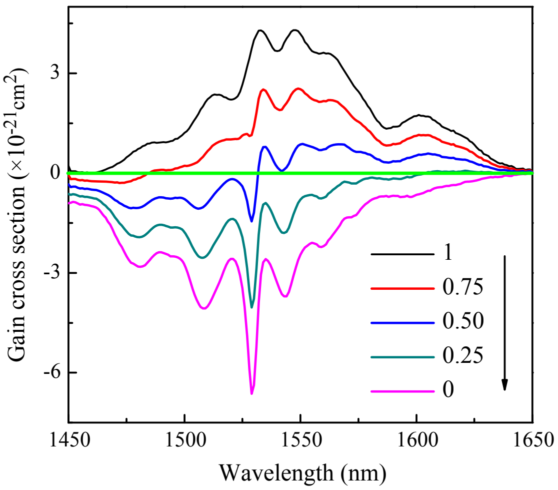

Fig. 8. Gain cross-section spectra for the $^4I_{13/2}\rightarrow{}^4I_{15/2}$ transition of Er^{3+} ion as a function of the inverted population rate P.

Fig. 8 illustrates the gain cross-section of $^4I_{13/2}\rightarrow{}^4I_{15/2}$ transition in Zr/Er/Yb:LN crystal as a function of P ranging from 0 to 1, which is calculated by using the obtained absorption and emission cross-sections [46].

$$g(\lambda)=P\sigma_{em}(\lambda)-(1-P)\sigma_{abs}(\lambda) \tag{14}$$

where P is the population inversion ratio of Er^{3+} ions, defined as the ratio of the electron population densities of $^4I_{13/2}$ to that of $^4I_{15/2}$ state. As P is equal to 0.75 in the gain cross-section spectra, the value of g (λ) achieves a positive value at 1484 nm. It can be seen that a relatively flat in the spectral range from 1549 nm to 1628 nm is observed at $P=0.5$, corresponding to the C-band communication.

4. Conclusions

In conclusion, Er/Yb:LiNbO$_3$ crystals tri-doped with different anti-photorefractive ions such as Zn^{2+}, In^{3+} and Zr^{4+} present the dissimilar optical characteristics of Er^{3+} ion. The green emitting $^4S_{3/2}/^2H_{11/2}$ states of Er^{3+} ion are populated by a three-photon process in Zn/Er/Yb:LN crystal. The introduction of Zn^{2+} ions leads to an increase of green UC emission and a decreased 1.54 μm emission, which arises from the efficient cross relaxation process $^4I_{11/2}+{}^4I_{11/2}\rightarrow{}^4F_{7/2}+{}^4I_{15/2}$ (Er). Similar to Zn^{2+} ion, In^{3+} ion affects the optical characteristics of Er^{3+} ion via tuning the occupancy of Er^{3+} ion in In/Er/Yb:LiNbO$_3$ crystal. The behavior that the formation of $Er_{Li}^{2+}-Er_{Nb}^{2-}$ ion pairs induced by In^{3+} ions increases the three cross relaxation processes ($^4I_{9/2}+{}^4I_{15/2}\rightarrow{}^4I_{13/2}+{}^4I_{13/2}$, $^4S_{3/2}+{}^4I_{15/2}\rightarrow{}^4I_{9/2}+{}^4I_{13/2}$ and $^4S_{3/2}+{}^4I_{15/2}\rightarrow{}^4I_{13/2}+{}^4I_{9/2}$) is contribution to the decreased green UC emission. The significantly enhanced 1.54 μm emission has been realized in Er/Yb:LiNbO$_3$ crystal tri-doped with

Zr^{4+} ions under 980 nm excitation. A fast nonradiative relaxation process of $^4I_{11/2}\rightarrow{}^4I_{13/2}$, arising from the increased OH$^-$ content, is responsible for the efficient 1.54 μm emission in Zr/Er/Yb:LN crystal. The J–O intensity parameters Ω_t (t=2, 4 and 6) of Zr/Er/Yb:LN crystal are calculated to be $\Omega_2=8.10\times10^{20}$ cm^2, $\Omega_4=3.72\times10^{20}$ cm^2 and $\Omega_6=1.28\times10^{20}$ cm^2, respectively. Zr/Er/Yb:LN crystal has the lengthening radiative lifetime (τ_{rad}) of $^4I_{13/2}$ state (Er) and the small fluorescence branching ratio (β) of $^4S_{3/2}\rightarrow{}^4I_{15/2}$ transition. These J–O intensity parameters suggest that the Zr^{4+} ion could be considered as an optimal anti-photorefractive ion in Er/Yb:LiNbO$_3$ crystal. The absorption/emission cross-sections and the gain cross-section show that Er/Yb:LiNbO$_3$ tri-doped with the anti-photorefractive ions would be the potential laser operation at around 1.54 μm emission.

Acknowledgments

We are grateful to the National Natural Science Foundation of China (Nos. 10732100, 11232015, 11072271 and 10972239) and the China Postdoctoral Science Foundation (No.:2012M521640).

References

[1] Wang HQ, Batentschuk M, Osvet A, Pinna L, Brabec CJ. Rare-earth ion doped up-conversion materials for photovoltaic applications. Adv Mater 2011;23:2675–80.

[2] Wild JD, Meijerink A, Rath JK, van Sark WGJHM, Schropp REI. Upconverter solar cells: materials and applications. Energy Environ Sci 2011;4:4835–48.

[3] Auzel F. Upconversion and anti-Stokes processes with f and d ions in solids. Chem Rev 2004;104:139–74.

[4] Polman A. Erbium implanted thin film photonic materials. J Appl Phys 1997;82:1–40.

[5] Zhang DL, Chen XJ, Wang YF, Zhu DS, Wu B, Lan GX. Influence of vapor transport equilibration on Raman spectra of Er:LiNbO$_3$ crystals. J Phys Chem Solids 2002;63:345–58.

[6] Zhang DL, Zhang P, Wong WH, Pun EYB. Locally Er-doped near-stoichiometric LiNbO$_3$ crystal for integrated optics. Cryst Growth Des 2008;8:2121–4.

[7] Sun L, Li AH, Guo FY, Lü Q, Xu YH, Zhao LC. Enhanced 1.5 μm emission and simultaneously suppressed green upconversion emission in Er:LiNbO$_3$ crystals heavily codoped with MgO. Appl Phys Lett 2007;91:0719141–3.

[8] Zhang DL, Wu C, Yang QZ, Sun L, Xu YH, Pun EYB. Transient characteristics of green upconversion emission of Er^{3+} in MgO:LiNbO$_3$ crystal: Mg threshold concentration effect. Appl Phys B 2009;95:335–40.

[9] Qian YN, Wang R, Xu C, Xing LL, Xu YL, Yang CH. Enhancement of 1.54 μm emission in Er:LiNbO$_3$ crystal by codoping with Zn^{2+} ions. J Rare Earths 2012;30:25–8.

[10] Sun L, Yang CH, Li AH, Xu YH, Zhao LC. In/Er-codoped LiNbO$_3$ crystals with enhanced 1.5 μm emission and suppressed upconversion emission. J Appl Phys 2009;105:0435121–6.

[11] Qian YN, Wang R, Xu C, Xu W, Wu XH, Xing LL, et al. The influence of Zn^{2+} ion on the 1.5 μm laser properties of LiNbO$_3$ crystal heavily doped with Er^{3+} ion. Opt Laser Technol 2012;44:2297–301.

[12] Li AH, Sun L, Zheng ZR, Wu WZ, Liu WL, Yang YQ, et al. Spectroscopic analysis of Er^{3+} transition in Mg/Er-codoped LiNbO$_3$ crystal. J Lumin 2008;128:239–44.

[13] Li AH, Sun L, Zheng ZR, Liu WL, Wu WZ, Yang YQ, et al. Spectroscopic properties of Er^{3+} in Sc:LiNbO$_3$ crystal. Appl Phys A 2007;89:1005–10.

[14] Li A, Sun L, Zheng Z, Lü Q, Wu W, Liu W, et al. Spectroscopic properties of Er^{3+} ions in LiNbO$_3$ crystals codoped with HfO$_2$. Appl Phys B 2008;90:29–34.

[15] Deng JC, Zhang WL, Wen JK, Zhang GY, Wang HF. Pulsed-laser-induced dark traces in LiNbO$_3$:Zn and LiNbO$_3$:Mg. Opt Lett 1994;19:933–5.

[16] Volk TR, Pryalkin VI, Rubinina NM. Optical-damage-resistant LiNbO$_3$:Zn crystal. Opt Lett 1990;15:996–8.

[17] Kong YF, Wen JK, Wang HF. New doped lithium niobate crystal with high resistance to photorefraction—LiNbO3. Appl Phys Lett 1995;66:280–1.

[18] Yan WB, Shi LH, Chen HJ, Zhang XZ, Kong YF. Investigations on the UV photorefractivity of LiNbO$_3$:Hf. Opt Lett 2010;35:601–3.

[19] Kong YF, Liu SG, Zhao YJ, Liu HD, Chen SL, Xu JJ. Highly optical damage resistant crystal: zirconium-oxide-doped lithium niobate. Appl Phys Lett 2007;91:0819081–3.

[20] Cantelar E, Muñoz JA, Sanz-García JA, Cusso F. Yb^{3+} to Er^{3+} energy transfer in LiNbO$_3$. J Phys: Condens Matter 1998;10:8893–903.

[21] Cantelar E, Cussó F. Analytical solution of the transfer rate equations in LiNbO$_3$:Er^{3+}/Yb^{3+}. J Phys: Condens Matter 2000;12:521–7.

[22] Qian YN, Wang R, Xu C, Wu XH, Xing LL, Xu YL. Optical spectroscopy and laser parameters of Zn^{2+}/Er^{3+}/Yb^{3+}-tridoped LiNbO$_3$ crystal. J Lumin 2012;132:1976–81.

[23] Qian YN, Wang R, Xu C, Xu W, Wu XH, Yang CH. Spectroscopic characteristics of 1.54 μm emission in Er/Yb:LiNbO$_3$ crystals tri-doped with In^{3+} ions. J Alloys Compd 2012;527:152–6.

[24] Joshi C, Rai RN, Rai SB. Structural, thermal, and optical properties of Er^{3+}/Yb^{3+} co-doped oxyhalide tellurite glasses, glass-ceramics and ceramics. J Quant Spectrosc Radiat Transfer 2012;113:397–404.

[25] Zheng KZ, Zhao D, Zhang DS, Liu N, Qin WP. Ultraviolet upconversion fluorescence of Er3+ induced by 1560 nm laser excitation. Opt Lett 2010;35:2442–4.

[26] Qian YN, Wang R, Xing LL, Xu YL, Yang CH, Liu XR. The effect of In^{3+} ion on the optical characteristics of Er^{3+} in Er/Yb:LiNbO$_3$ crystal. Opt Mater 2012;34:884–8.

[27] Wang X, Kong XG, Yu Y, Sun YJ, Zhang H. Effect of annealing on upconversion luminescence of ZnO:Er^{3+} nanocrystals and high thermal sensitivity. J Phys Chem C 2007;111:15119–24.

[28] Iyi N, Kitamura K, Izumi F, Yamamoto JK, Hayashi T, Asano H, et al. Comparative study of defect structures in lithium niobate with different compositions. J Solid State Chem 1992;101:340–52.

[29] Hehlen MP, Cockroft NJ, Gosnell TR, Bruce AJ. Spectroscopic properties of Er^{3+}- and Yb^{3+}-doped soda-lime silicate and aluminosilicate glasses. Phys Rev B 1997;56:9302–18.

[30] Saleem SA, Jamalaiah BC, Jayasimhadri M, Rao AS, Jang KW, Moorthy LR. Luminescent studies of Dy^{3+} ion in alkali lead tellurofluoroborate glasses. J Quant Spectrosc Radiat Transfer 2011;112:78–84.

[31] Babu YNChRavi, Naik PSR, Kumar KV, Kumar NR, Kumar AS. Spectral investigations of Sm^{3+} doped lead bismuth magnesium borophosphate glasses. J Quant Spectrosc Radiat Transfer 2012;113:1669–75.

[32] Lomheim TS, DeShazer LG. Optical-absorption intensities of trivalent neodymium in the uniaxial crystal yttrium orthovanadate. J Appl Phys 1978;49:5517–23.

[33] Weber MJ. Probabilities for radiative and nonradiative decay of Er^{3+} in LaF$_3$. Phys Rev 1967;157:262–72.

[34] Schlarb U, Betzler K. Refractive indices of lithium niobate as a function of temperature, wavelength, and composition: a generalized fit. Phys Rev B 1993;48:15613–20.

[35] Amin J, Dussardier B, Schweizer T, Hempstead M. Spectroscopic analysis of Er^{3+} transitions in lithium niobate. J Lumin 1996;69:17–26.

[36] Bertini C, Toncelli A, Tonelli M, Cavalli E, Magnani N. Optical spectroscopy and laser parameters of GdVO4:Er^{3+}. J Lumin 2004;106:235–42.

[37] Lisiecki R, Dominiak-Dzik G, Solarz P, Strzep A, Ryba-Romanowski W, Łukasiewicz T. Spectroscopic characterisation of Er-doped LuVO$_4$ single crystals. Appl Phys B 2010;101:791–800.

[38] Dong Q, Zhao GJ, Cao DH, Chen JY, Ding YC. Growth and anisotropic spectral properties of Er:YAlO$_3$ crystal. J Alloys Compd 2010;493:661–5.

[39] Ding YC, Zhao GJ, Xu XD. Crystal growth and spectroscopic properties of erbium doped Lu$_2$SiO$_5$. J Cryst Growth 2010;312:2103–6.

[40] Pujol MC, Rico M, Zaldo C, Solé R, Nikolov V, Solans X, et al. Crystalline structure and optical spectroscopy of Er^{3+}-doped KGd(WO$_4$)$_2$ single crystals. Appl Phys B 1999;68:187–97.

[41] Tian Y, Xu RR, Hu LL, Zhang JJ. 2.7 μm fluorescence radiative dynamics and energy transfer between Er^{3+} and Tm^{3+} ions in fluoride glass under 800 nm and 980 nm excitation. J Quant Spectrosc Radiat Transfer 2012;113:87–95.

[42] McCumber DE. Einstein relations connecting broadband emission and absorption spectra. Phys Rev 1964;134:954–7.

[43] Xie JH, Zhang Q, Zhuang YX, Liu XF, Guan MJ, Zhu B, et al. Enhanced mid-IR emission in Yb^{3+}-Tm^{3+} co-doped oxyfluoride glass ceramics. J Alloys Compd 2011;509:3032–7.

[44] Sokólska I. Spectroscopic characterisation of LaGaO3:Er^{3+} crystals. Appl Phys B 2000;71:157–62.

[45] Zhao D, Wang GF. Growth and spectroscopic characterization of Er^{3+}: $Sr_3Y(BO_3)_3$ crystal. J Lumin 2010;130:424–8.

[46] Hömmerich U, Hanley C, Brown E, Trivedi SB, Zavada JM. Spectroscopic studies of the 1.5 μm (4I15/2 → 4I13/2) emission from polycrystalline ceramic Er:YAG and Er:KPb_2Cl_5. J Alloys Compd 2009;488:624–7.